Self-oscillations in spin-wave instabilities

S. M. Rezende and A. Azevedo
Departamento de Física, Universidade Federal de Pernambuco, 50739 Recife, Brazil
(Received 20 September 1991)

An experimental and theoretical study of bifurcations leading to self-oscillations in spin-wave instabilities pumped by microwave fields is presented. The experiments were done with spheres of yttrium iron garnet of various diameters pumped by X-band microwave radiation in the parallel pumping and subsidiary resonance configurations. The results reveal a variety of bifurcations and chaos depending on the experimental parameters. Generally the frequency and threshold of the self-oscillations show a definite dependence on sample size not predicted by the existing models. On the theoretical side we show that the usual equations describing two interacting spin-wave modes predict various types of bifurcations, depending on the set of parameters. In particular we investigate Hopf bifurcations and homoclinic phenomena. We also show that the introduction of boundary conditions and momentum symmetry breaking in the spin-wave pumping in finite samples accounts for important quantitative features of the experimental observations not explained by the existing models.

I. INTRODUCTION

In a magnetic material subjected to microwave radiation, the rf magnetic field can drive spin waves by means of several parametric processes.[1-5] Nonlinear spin-wave excitation occurs when the microwave power exceeds the so-called Suhl instability (SI) threshold, which depends on the pumping configuration, material parameters, and the value of the static applied field. Since the early days of spin-wave pumping experiments, it has been known that as the rf field is increased beyond the SI threshold, the radiation absorbed by the sample spontaneously develops low-frequency (10 kHz–1 MHz) oscillations.[6] Only recently, the mechanisms responsible for these so-called auto-oscillations have been better understood in the light of the theory of bifurcations in nonlinear dynamics. However, despite the recent progress, major quantitative discrepancies remain between theory and experiment. The aim of the present paper is to resolve these discrepancies.

Nonlinear behavior in ferromagnets was first observed in microwave magnetic-resonance experiments in the early 1950s. Damon[1] and Bloembergen and Wang[2] observed a premature saturation of the main resonance absorption and the appearance of a subsidiary absorption when the microwave power exceeded certain threshold levels. A few years later, Suhl[3] produced a theory to explain those intriguing observations based on the parametric generation of spin waves. Later, it was predicted[4,5] that spin waves could also be parametrically pumped by a microwave field parallel to the dc magnetic field $\mathbf{h}\|\mathbf{H}_0$. This was called the parallel-pumping process to distinguish from the perpendicular-pumping Suhl processes observed in the magnetic-resonance configuration ($\mathbf{h}\perp\mathbf{H}_0$). In all three parametric processes, the SI threshold h_c for pumping a given spin-wave mode is determined by the rate at which energy must be pumped into that mode to overcome the power dissipated to the lattice. Since both the coupling to the microwave field and the relaxation rate depend on the wave vector $\mathbf{k}$, there is a certain mode for which the threshold attains a minimum value $h_c^{\min}$. Increasing the microwave field beyond this value results in the excitation of many other modes, but initially the system remains in steady state. Only when the field exceeds a second threshold h_c' do the auto-oscillations break in. The frequencies of these oscillations are in the range 10 kHz–1 MHz and bear no relation to the microwave pumping frequency 1–10 GHz.

The threshold, frequency, and wave shape of the auto-oscillations depend on the pumping configuration, dc-field value H_0, crystal-axis orientation with respect to $\mathbf{H}_0$, and also on sample shape, dimensions, surface polishing, and temperature. Over the years, several explanations were proposed for the origin of the auto-oscillations. The most noticeable prenonlinear dynamics model was proposed by Thomas and co-workers.[7,8] According to their model, because of the finite linewidth of the spin waves, several modes with spread Δk in wave number and $\Delta\omega_k$ in frequency are excited above the SI threshold. The beat between these modes would produce an auto-oscillation with frequency $\Delta\omega = v_g \Delta k$, so that it is determined by the boundary conditions via $\Delta k \approx \pi/d$ (d is the sample dimension along the propagation direction) and by the group velocity $v_g = \partial\omega_k/\partial k$. This model explained some features of the experimental data, such as the dependence of the frequency on H_0 and on sample dimensions. However, it completely failed in explaining the nature of the auto-oscillation threshold and the dependence of the frequency on the pump power, above h_c'. This was noted by L'vov and co-workers and others,[9] who were the first to recognize the nonlinear nature of the phenomenon. They established that the auto-oscillations arise from the back-and-forth dynamic power exchange between parametric modes caused by their nonlinear coupling, but the quantitative results of their model were unsatisfactory.

In recent years the interest in spin-wave chaotic phe-

nomena has revived the investigations on the auto-oscillations, both theoretically and experimentally.[10–28] Most theoretical treatments have relied on computer numerical solutions of the nonlinear spin-wave equations derived from the model Hamiltonian introduced by Zakharov, L'vov, and Starobinets.[9] The numerical approach[10,13,14,19,26] requires the model to be restricted to a few spin-wave modes, ignoring the fact that in general a whole manifold of modes is excited above the threshold h_c. Experimentally, this problem has been circumvented by McMichael and Wigen[25] by using a very thin magnetic garnet film conveniently oriented in the static field. In this case only a few spin-wave modes are excited and good quantitative agreement is obtained between the predictions of the model and the measured auto-oscillation frequencies and threshold fields. In bulk samples the situation is much more complex because an almost continuum of modes is excited. However, recently, Suhl and Zhang[17] have shown that the dynamics is effectively governed by two modes, the one with strongest coupling to the pump and a normal mode resulting from the collective rearrangement of all the other modes. This result provides a formal justification for the use of the two-mode model successfully[13,14,19,24,26] employed to interpret qualitatively the experimental data in bulk samples. Despite the continuing progress, the numerical treatments as well as the theory of Suhl and Zhang invariably predict auto-oscillation thresholds and frequencies quite larger than the experimentally observed ones. Moreover, none of the nonlinear-dynamics calculations explains the sample-size dependence of the frequency observed in some experiments.[8,11,27,28]

In this paper we present an experimental and theoretical investigation of the auto-oscillations in spin-wave instabilities generated either in parallel-pumping or subsidiary-resonance configurations. The experiments were done with yttrium iron garnet (YIG) spheres of various diameters to obtain a large set of data to compare with theory.

In Sec. II we describe the experiments and give some background information about spin-wave pumping. Section III presents details for the bifurcations leading to self-oscillations and data for the dependence of the frequency and threshold on the wave number k and sample size. Section IV is devoted to the theoretical model, which is restricted to plane spin waves with wavelength much shorter than the sample size. We show how the finite size of the sample gives rise to a momentum symmetry breaking in the spin-wave pumping, which adds another term in the equations governing the dynamics. The numerical solutions of the nonlinear equations for two modes and comparison with the data are explored in Secs. V and VI. Section VII presents the conclusions. A preliminary account of this work has been published elsewhere.[28]

II. EXPERIMENTAL EXCITATION OF SPIN-WAVE INSTABILITIES

A. Experimental setup

The experiments were performed at room temperature with polished single-crystal YIG spheres of various diameters. The sample is located at the center of a critically coupled rectangular TE_{102} microwave cavity with $Q \simeq 2000$, placed between the poles of an electromagnet that provides the static field $\mathbf{H}_0$. The cavity can be oriented so that the microwave magnetic field $\mathbf{h}$ is either parallel or perpendicular (subsidiary resonance) to $\mathbf{H}_0$. The microwave radiation is generated by a X-band backward-wave oscillator (BWO) and amplified to 1.8 W by a traveling-wave tube (TWT). The BWO frequency is stabilized by an external crystal oscillator and manually adjusted to the center of the cavity resonance. The radiation power is then controlled with a variable precision attenuator and directed by a circulator to the resonant cavity, where it drives spin waves in the sample. The reflected microwave signal is detected with a sensitive Schottky-barrier diode at the output port of the circulator and recorded in a digital storage oscilloscope. In order to avoid sample heating, the microwave radiation is pulsed (duration 100 μsec at 100 pulses/sec) with a p-i-n modulator placed before the TWT amplifier. This causes no difficulty for recording the steady-state regime of the sample response because the transient time is normally much shorter than the pulse length.

B. Spin-wave parametric processes

At low-power levels the pulse reflected from the cavity has essentially the same shape as the incoming microwave pulse. As the power is increased, an abrupt change in the pulse shape occurs when the driving field h reaches the minimum threshold $h_c^{\min}$ for spin-wave parametric excitation. Spin waves are excited in pairs with wave vectors $\pm\mathbf{k}$ and nearly half the microwave pumping frequency, $\omega_k \simeq \omega_p/2$. The spin-wave pair establishes a standing-wave mode, and because of the boundary conditions, only discrete resonating modes are excited. So, in general, the spin-wave frequency differs slightly from the half-pumping frequency by a detuning parameter $\Delta\omega_k = \omega_k - \omega_p/2$. As we shall see later, although the detuning is small ($\Delta\omega_k/\omega_k \sim 10^{-4}$), it plays a very important role in the connection between the auto-oscillation frequency and sample size. The wave vectors $\pm\mathbf{k}$ of the pair are determined by the frequency ω_k, the field H_0, and the condition for minimum threshold. If H_0 is applied along a crystal direction of high symmetry, the spin-wave dispersion relation for $k \ll 10^7$ cm^{-1} is[3]

$$\omega_k = \gamma(H_z + H_A + Dk^2)^{1/2} \times (H_z + H_A + Dk^2 + 4\pi M \sin^2\theta_k)^{1/2}, \quad (1)$$

where $H_z = H_0 - 4\pi M N_z$, N_z is the demagnetizing factor in the (z) direction of the external dc field $\mathbf{H}_0$, $\gamma = g\mu_B/\hbar$ is the gyromagnetic ratio, M is the saturation magnetization, θ_k is the angle between $\mathbf{k}$ and $\mathbf{H}_0$, D is the exchange stiffness, and H_A is the effective magnetic anisotropy field. In pure YIG, [111] is the easy axis, $H_A \simeq 60$ Oe, $D = 5.4 \times 10^{-9}$ Oe cm^2, $4\pi M = 1760$ Oe at room temperature, and $\gamma = 2.8$ GHz/kOe or 17.6×10^6 sec^{-1}/Oe.

The spin-wave threshold field is given by[4,5,26]

$$h_c = \frac{(\gamma_k^2 + \Delta\omega_k^2)^{1/2}}{|\rho_k|} , \tag{2}$$

where γ_k is the relaxation rate and ρ_k represents the coupling between the pumping field and spin-wave mode. The relaxation rate varies linearly with k ($\gamma_k \simeq \gamma_0 + bk$) and is of the order of 10^6 sec^{-1} in YIG in the frequency range of our experiments.

In the parallel-pumping process,[4,5] the $k \simeq 0$ microwave field h couples directly to a $\pm\mathbf{k}$ magnon pair with frequency $\omega_k \approx \omega_p/2$, as illustrated in Fig. 1(a). This is due to the ellipticity in the spin precession arising from the dipolar interaction, giving a coupling factor in the form[4,5,26]

$$\rho_k = \gamma\omega_M \sin^2\theta_k e^{-i2\varphi_k}/4\omega_k , \tag{3}$$

where θ_k and φ_k are the polar and azymuthal angles of $\mathbf{k}$ with respect to $\mathbf{H}_0$ and $\omega_M = \gamma 4\pi M$. Note that the coupling is strongest for spin waves propagating perpendicularly to $\mathbf{H}_0$. Hence this is the mode with minimum threshold in the range $H_0 < H_c$, where H_c is the field for which the dispersion relation (1) gives $\omega_k = \omega_p/2$ for $\theta_k = \pi/2$, $k = 0$. In YIG, $\omega_M \sim \omega_k$ for X-band pumping, so that the minimum threshold from (2) is $h_c^{\min} \sim 4\gamma_k/\gamma \sim 10^{-1}$ Oe.

In the perpendicular-pumping configuration, the microwave field couples linearly to the uniform mode ($k = 0$) and one observes a ferromagnetic resonance (FMR) absorption at $H_0 \simeq \omega_p/\gamma$. Although spin waves with $k \neq 0$ do not couple directly to the radiation, they can be excited via magnon-magnon interactions.[3] In the first-order Suhl process, spin waves with $\omega_k \simeq \omega_p/2$ in a $\pm\mathbf{k}$ pair can be driven parametrically by the uniform mode by means of a three-magnon interaction, as shown in Fig. 1(b). Since the uniform mode couples very strongly to the pumping field, it can be driven far off resonance with frequency $\omega \approx \omega_p/2$ and excite spin waves. So, when the pumping exceeds the threshold $h_c^{\min}$, one observes a *subsidiary resonance* at a field H_0 roughly half the value for the main resonance. In this case the threshold is also given by Eq. (2) with a coupling factor[26]

$$\rho_k \simeq \gamma\omega_M \sin 2\theta_k e^{-i\varphi_k}/4\omega_k . \tag{4}$$

Hence, at the end, the subsidiary resonance process is very similar[19,26] to parallel pumping and the minimum threshold is also $h_c^{\min} \sim 4\gamma_k/\gamma \sim 10^{-1}$ Oe in YIG. The main difference to parallel pumping is that the mode with minimum threshold for $H_0 < H_c$ has $\theta_k = \pi/4$ instead of $\pi/2$, as illustrated in Fig. 1(b).

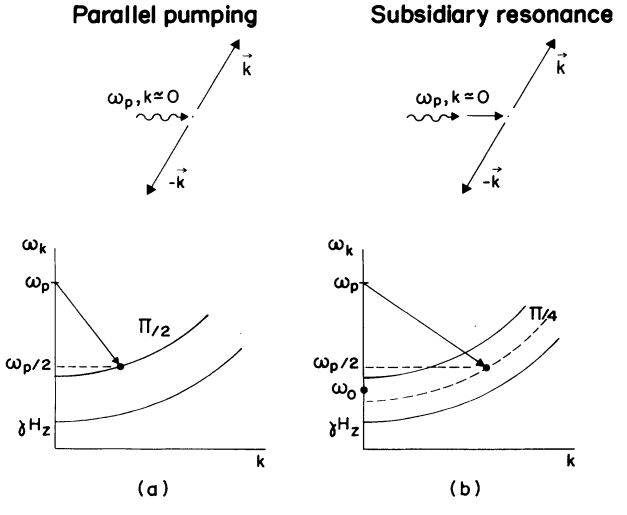

FIG. 1. Illustrations of spin-wave parametric pumping processes. (a) Parallel pumping. (b) Perpendicular pumping, subsidiary resonance (first-order Suhl process).

A third parametric process, which will not be studied here, is the premature saturation of the main resonance. In the perpendicular geometry, as the microwave power is increased, the absorption at the ferromagnetic resonance field $H_0 = \omega_0/\gamma \approx \omega_p/\gamma$ stops increasing when a threshold is reached. This results from the parametric pumping of a spin-wave pair by two uniform-mode magnons with frequency $\omega_0 \approx \omega_p \approx \omega_k$, through the four-magnon interaction in the so-called second-order Suhl process.[3] The threshold field in this case is $\sim 10^{-3}$ Oe in YIG, and no resonant cavity is needed to observe it in bulk samples.

III. ONSET OF AUTO-OSCILLATIONS

A. Phase boundaries

As the microwave power is increased beyond the Suhl threshold, the signal reflected from the cavity-sample system spontaneously develops a low-frequency amplitude modulation. This occurs at a threshold $h_c' > h_c$ and is associated with a bifurcation in the response of the nonlinear spin-wave system. A bifurcation is the analog of a phase transition in equilibrium thermodynamics and corresponds to a qualitative change in the dynamic state of the system as some relevant parameter is varied. Figure 2 shows the phase boundaries measured with parallel pumping at $f_p = \omega_p/2\pi = 9.5$ GHz in a 1-mm YIG sphere aligned with the [111] axis along $\mathbf{H}_0$. The lower boundary characterizes the bifurcation leading to the spin-wave instability (h_c). It is the familiar "butterfly curve," featuring a sharp minimum at the field $H_0 = H_c \simeq 1540$ Oe for which the $\theta_k = \pi/2$ mode has minimum damping at $k = 0$. The upper boundary corresponds to the auto-oscillation bifurcation (h_c'). Throughout the whole field range, the self-oscillation sets in with a finite frequency $f_0 = 50$–1000 kHz and vanishing amplitude. This is a characteristic feature of a Hopf bifurcation. Beyond the threshold h_c', the oscillation amplitude grows rapidly while the frequency increases smoothly with pumping field. The inset of Fig. 2 shows the variation of f_0 with h for $H_0 \simeq H_c = 1540$ Oe. Note that at the onset the auto-oscillation frequency is of order $f_0 \sim 10^{-1}\gamma_k$ and the threshold h_c' is only a few db above h_c. This is in contradiction with the theory of Suhl and Zhang[17] and the results of computer simulations (Refs. 10, 13, 14, 19, 24, and 26), which predict $f_0 \sim \gamma_k$ and h_c' in excess of h_c by as much as 10 db.

The gross features of the spin-wave instabilities driven

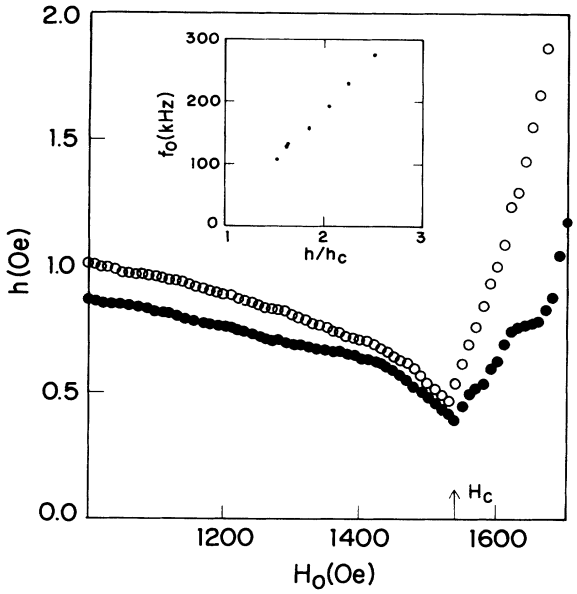

FIG. 2. Threshold field for spin-wave instability h_c (●) and for auto-oscillation h_c' (○) in a 1-mm YIG sphere under parallel pumping at $f_p=9.5$ GHz. The sample is oriented with the [111] axis along $\mathbf{H}_0$. The inset shows the auto-oscillation frequency vs pumping field at $H_0=1540$ Oe.

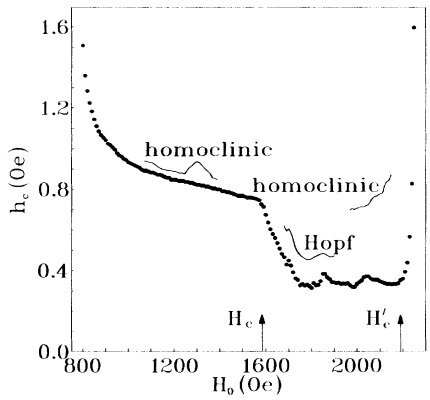

FIG. 3. Threshold fields for spin-wave instability h_c (●) and for auto-oscillation h_c' (solid lines) in a 1-mm YIG sphere under subsidiary-resonance pumping at $f_p=8.87$ GHz. The sample is oriented with the [110] axis along $\mathbf{H}_0$.

in subsidiary resonance are similar to those in parallel pumping. Figure 3 shows the phase boundaries for spin-wave excitation and auto-oscillation measured in the same 1-mm YIG sphere of Fig. 2, with H_0 along the [110] axis and microwave frequency 8.87 GHz. Instead of a sharp minimum, the butterfly curve for subsidiary resonance has a broad minimum and three characteristic regions in field H_0. For $H_0<H_c\simeq 1580$ Oe, the modes with lowest threshold are plane waves with $k>0$ propagating at an angle $\theta_k=\pi/4$ with $\mathbf{H}_0$ (or $\theta_k\simeq 35°$ depending on the effect of the relaxation rate[29]). For $H_c<H_0<H_c'=2190$ Oe, the modes with minimum threshold are magnetostatic waves with $k\approx 0$. For $H_0>H_c'$ the threshold rises sharply with H_0 as $\theta_k\to 0$. Since in the various field regions the modes excited have different nonlinear coupling parameters, a variety of bifurcations leading to self-oscillations can be observed at different field values, as indicated on the boundary lines for self-oscillation in Fig. 3.

B. Critical behavior

The behavior of the frequency and amplitude of the self-oscillations near the threshold depends strongly on the type of bifurcation. Analogously to what happens in phase transitions in equilibrium thermodynamics, the critical behavior of these quantities can be characterized by scaling laws and critical exponents. Figure 4 shows the growth of the auto-oscillation with increasing pumping in the parallel configuration of Fig. 2 at $H_0=1570$ Oe. The detailed data for the amplitude A and frequency f_0 as a function of the reduced driving field $r=h/h_c'-1$ in the critical region is shown in Fig. 5. The data reveal the scaling behavior in the critical region $f_0\sim r^{\alpha}$ and $A\sim r^{\beta}$, where $\alpha=0$ and $\beta=0.5$. These exponents are characteristic features of a Hopf bifurcation.[30] This type of bifurcation is the most commonly observed in spin-wave instabilities, but contrary to the usual assertion,[17,19] it is not the only one. In fact, in subsidiary-resonance pumping with $\mathbf{H}_0$ along the [110] axis of the YIG sphere, as indicated in Fig. 3, it is more common to find another type of bifurcation, which we have identified as a homoclinic one. This is illustrated in Fig. 6, which shows the auto-oscillation for several values of $h\geq h_c'$ with $H_0=1950$ Oe. In this case the auto-oscillation sets in with vanishing frequency and finite amplitude. Near the threshold the oscillation is somewhat aperiodic, but as the field increases, it becomes periodic with increasing frequency and constant amplitude, just the opposite of the scenario in the Hopf case.

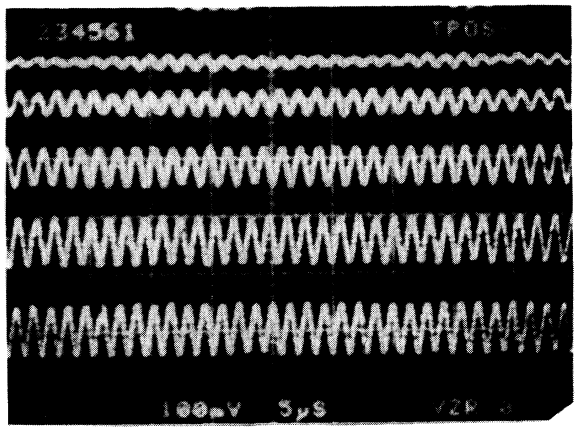

FIG. 4. Oscilloscope traces showing the behavior of the auto-oscillation with increasing microwave field $R=h/h_c$ in parallel pumping with a YIG sphere oriented along [111], $H_0=1570$ Oe, $f_p=9.5$ GHz. The time scale is 5 μs per division, and $R=1.224$, 1.255, 1.293, 1.321, and 1.342 from top to bottom. The constant frequency and rapid growth in the amplitude characterize a Hopf bifurcation.

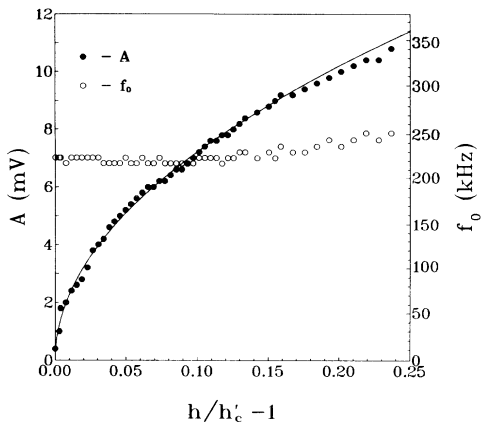

FIG. 5. Data for the auto-oscillation amplitude A and frequency f_0 vs reduced pumping $r=h/h_c'-1$ near the bifurcation for the same condition of Fig. 4, with $H_0=1620$ Oe. The solid line is a fit to $A \propto r^{1/2}$.

C. Sample-size dependence

In the early investigations of auto-oscillations, it was observed that the frequency presented a marked dependence on sample size.[7,8] In one of the first papers on nonlinear dynamics in the recent upsurge of interest on spin-wave instabilities, Gibson and Jeffreys[11] noted the existence of two auto-oscillation frequencies in perpendicular pumping in a 1-mm sphere of Ga-YIG, $f_{A1}=250$ kHz and $f_{A2}=16$ kHz. They did call attention for the size dependence of f_{A1}, but perhaps because the interesting chaotic dynamics occurred in the f_{A2} mode, not much attention was paid to f_{A1}. We have investigated this point in detail. Depending on the pumping configuration and sample shape, the auto-oscillation frequency and threshold may present a clear dependence on sample size. Figure 7 shows the data for parallel pumping in YIG spheres with diameters $d=0.52$ and 1.0 mm aligned along the [111] axis. Figures 7(a) and 7(b) show the threshold fields for spin-wave instability (h_c) and auto-oscillation (h_c'), while Figs. 7(c) and 7(d) display the corresponding threshold frequencies versus H_0. Clearly, both the frequency and threshold difference $h_c'-h_c$ scale with the diameter roughly as $1/d$.

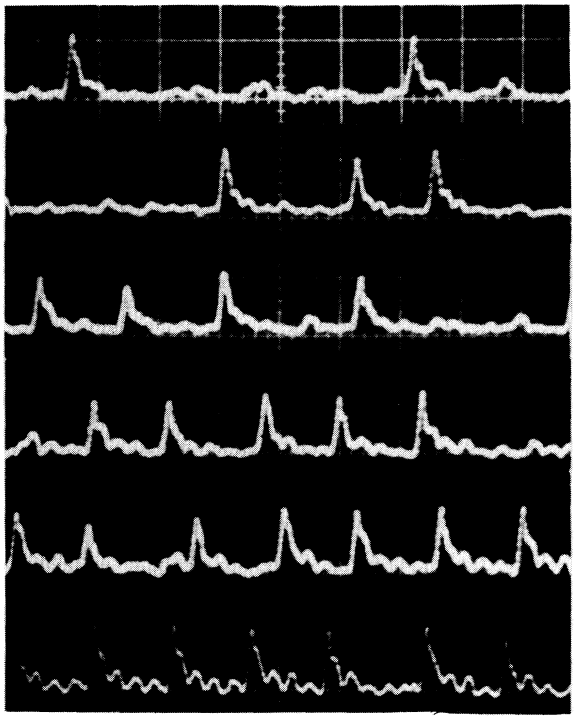

FIG. 6. Oscilloscope traces of the auto-oscillation obtained with subsidiary-resonance pumping with increasing microwave field $R=h/h_c$ in a YIG sphere oriented along [110], $H_0=1950$ Oe, $f_p=9.4$ GHz. The time scale is 10 μs per division $R=1.862$, 1.872, 1.883, 1.894, 1.905, and 1.916 from top to bottom. Note that the auto-oscillation sets in with a finite amplitude and rapidly increasing frequency, quite differently from the Hopf scenario of Fig. 4.

In order to compare the data of Fig. 7 with the theory to be developed in the next sections, we express the frequency as a function of the wave number k of the modes involved. For this we consider only the field range $H_0<H_c$ since the mode excited first has the same angle $\theta_k=\pi/2$ and varying k. Since $h_c'\geq h_c$, we assume further that the modes involved in the auto-oscillation also have $\theta_k\simeq\pi/2$. So the measurement of the threshold frequency f_0 as a function of H_0 can be expressed in terms of k using Eq. (1). The relaxation rate γ_k versus k can also be determined from the h_c data of Fig. 7 with Eqs. (2) and (3). Figure 8 shows the measured ratio f_0/γ_k (f_0 in Hz and γ_k in $\sec^{-1}$) at the bifurcation as a function of k for the $\pi/2$ mode for three spheres with diameters 0.52, 1.00, and 2.00 mm. The data show clearly that the frequency is not given by the simple theoretical prediction[17] $f_0\sim 2\gamma_k$. In fact, the ratio f_0/γ_k varies with wave number k in a linear fashion in the field range of the data.

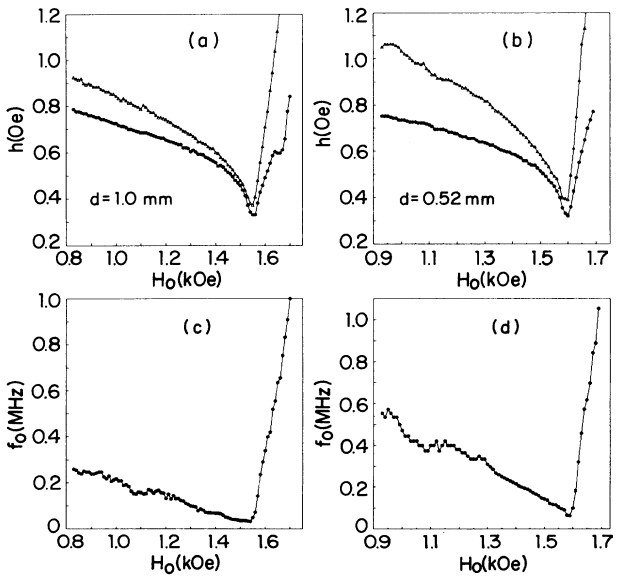

FIG. 7. Data for the auto-oscillation frequency f_0 and threshold fields for two YIG spheres with diameters 1.0 mm (left) and 0.52 mm (right) obtained with parallel pumping at $f_p\simeq 9.5$ GHz. Both results were obtained with the [111] axis along $\mathbf{H}_0$.

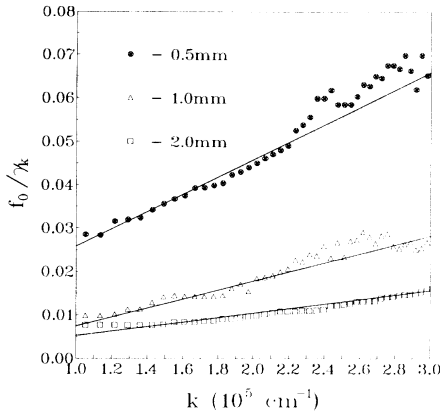

FIG. 8. Ratio of the auto-oscillation frequency f_0 to the relaxation rate γ_k at the bifurcation, as a function of k for various YIG spheres in parallel pumping. The solid lines are fits to $f_0/\gamma_k = a + bk/d$, where d is the sphere diameter; $b = 0.0104$, and $a = 0.0058$, -0.003, and 0.00 for $d = 0.52$, 1.0, and 2.0 mm, respectively.

Most interestingly, f_0/γ_k, as well as the threshold field h_c', has a marked dependence on sample diameter. These results, not predicted by existing theories of the auto-oscillation, are explained by the model presented in the next section.

IV. THEORETICAL MODEL

The nonlinear differential equations that govern the dynamics of large-k, plane spin-wave instabilities have been derived by many authors. In all approaches the interacting spin-wave system is considered to be driven by a uniform microwave field in such a way that the pumping term of the Hamiltonian conserves momentum; i.e., magnons are generated in pairs $\pm\mathbf{k}$. This is strictly correct only for an infinite medium; hence it cannot predict a sample-size dependence for the self-oscillation frequency and threshold. In this section we show that a non-momentum-conserving term is necessary to describe the spin-wave pumping in finite samples. In the numerical solutions of Sec. VI, we will show that the presence of this term also resolves the main defficiencies of the previous theoretical predictions, namely, too high frequencies and auto-oscillation thresholds.

We consider a spin-wave system described by the magnon creation and annihilation operators $c_k^\dagger$ and c_k. The expectation value of the magnon operator $\langle c_k^\dagger \rangle$ is proportional to the transverse-precessing magnetization $m^+ = m_x + im_y$. Since m^+ gives the transverse (circularly polarized) microwave susceptibility of the sample, it is related to the amplitude-modulation signal in the subsidiary-resonance experiment. In the parallel-pumping configuration, the signal is related to the z component of the magnetization and thus to the magnon occupation number $n_k = \langle c_k^\dagger c_k \rangle$. The Hamiltonian for a spin-wave system pumped by a microwave field can be written as[3,9,10,19,20,26]

$$\mathcal{H} = \mathcal{H}^{(2)} + \mathcal{H}^{(4)} + \mathcal{H}'(t) , \tag{5}$$

where

$$\mathcal{H}^{(2)} = \sum_k \hbar\omega_k c_k^\dagger c_k \tag{6}$$

is the Hamiltonian for a system of independent harmonic oscillators (magnons) with frequency ω_k, $\mathcal{H}^{(4)}$ represent the four-magnon interaction, and $\mathcal{H}'(t)$ describes the interaction with the microwave field. The essential ingredient for the nonlinear dynamics is the coupling between two pairs of parametric magnons provided by the four-magnon interaction. This has relevant terms of the form[9,10,19,20,26]

$$\mathcal{H}^{(4)} = \hbar \sum_{k,k'} \left(\tfrac{1}{2} S_{kk'} c_k^\dagger c_{-k}^\dagger c_{k'} c_{-k'} + T_{kk'} c_k^\dagger c_{k'}^\dagger c_k c_{k'} \right) . \tag{7}$$

In simple ferromagnets this interaction arises from the dipolar, anisotropy, and exchange energies, but the latter is negligible for the small k values excited in the microwave experiments. The interaction (7) couples the equations of motion for different k modes, giving rise to a variety of nonlinear behavior. The pumping term $\mathcal{H}'(t)$ has the same form in parallel and subsidiary-resonance pumpings,[19,26] even though the mechanisms by which photons are converted into magnons are different in the two cases. For a uniform microwave pumping field $h\exp(-i\omega_p t)$, it can be shown that

$$\mathcal{H}'(t) \simeq \tfrac{1}{2} h \sum_{k,k'} \hbar\rho_k e^{-i\omega_p t} c_k^\dagger c_{-k}^\dagger \Delta_{kk'} + \text{H.c.} , \tag{8}$$

where ρ_k is given by Eq. (3) or (4), depending on the pumping process, and $\Delta_{kk'} = N^{-1}\sum_i \exp[i(\mathbf{k}-\mathbf{k}')\cdot\mathbf{r}_i]$ is a sum over N lattice sites $\mathbf{r}_i$. In an infinite medium, $N \to \infty$, $\Delta_{kk'} \to \delta_{kk'}$ so that magnon pairs with wave vectors $\pm\mathbf{k}$ are driven by $k = 0$ photons in a momentum-conserving process. However, in a finite sample, $\Delta_{kk'}$ can be nonzero for $\mathbf{k} \neq \mathbf{k}'$. The type of standing waves set up in the sample and the exact form of $\Delta_{kk'}$ depend on the sample shape. For a parallelopiped with thicknesses L_x, L_y, L_z and N_x, N_y, N_z lattice sites along the three Cartesian directions, $\Delta_{kk'}$ can be written as the product of three terms of the type

$$N_x^{-1} \sum_{i_x} e^{i\Delta k_x x_i} = N_x^{-1} \frac{\sin(\Delta k_x a N_x/2)}{\sin(\Delta k_x a/2)} , \tag{9}$$

where a is the lattice parameter and $\Delta k_x = k_x - k_x'$. Boundary conditions require that $\Delta k_x = n_x(\pi/L_x)$, so that the sum (9) is $1, 2/\pi, 0, 2/3\pi, \ldots$ for $n_x = 0, 1, 2, 3, \ldots$, respectively. Therefore the driving term of the Hamiltonian becomes

$$\mathcal{H}'(t) \simeq \tfrac{1}{2} h \sum_{k,k'} \hbar\rho_k e^{-i\omega_p t} c_k^\dagger c_{-k}^\dagger \times (\delta_{kk'} + \alpha_{\Delta k}\delta_{k,k'\pm\Delta k} + \cdots) + \text{H.c.} , \tag{10}$$

where $\alpha_{\Delta k}$ is a factor which depends on the wave-vector mismatch $\Delta k_x, \Delta k_y, \Delta k_z$. For two neighboring standing waves along x (or y or z) with $\Delta k_x = \pi/L_x$, $\alpha_{\Delta k}$ attains its maximum value of $2/\pi$. In an infinite medium, $\alpha_{\Delta k} = 0$,

so that Eq. (10) reduces to the expression used in all treatments of spin-wave parametric pumping. Because of the presence of the symmetry-breaking term in a finite sample, the microwave field can drive directly two neighboring standing-wave modes with wave numbers k_1 and $k_2=k_1\pm\Delta k$, satisfying the energy-conservation relation $\omega_{k1}+\omega_{k2}=\omega_p$. This introduces an additional pumping term in the spin-wave equations for two neighboring modes.

When the pumping field exceeds the SI threshold, many $\mathbf{k}$ modes are excited. The equations of motion for the interacting spin waves are obtained from the Heisenberg equation for the magnon operator c_k using the Hamiltonian (5) and introducing dissipation phenomenologically. Since the spin waves are excited in pairs forming standing waves, one can assume[19] that $c_{-k}=\exp(iq_k)c_k$, where q_k is a real phase. Taking the expectation value of the magnon operator and introducing the slowly varying amplitude

$$\bar{c}_k=\langle c_k\rangle e^{iq_k/2}e^{i(\omega_p/2)t}, \tag{11}$$

we obtain the following equation of motion for the variable $\bar{c}_k$ that characterizes the spin-wave pair mode:

$$\frac{d\bar{c}_k}{dt}=-(\gamma_k+i\,\Delta\omega_k)\bar{c}_k-ih\rho_k(\bar{c}^{\,*}_k+\alpha_{\Delta k}\bar{c}^{*}_k e^{i\beta_{kk'}/2}) -i\sum_{k'}(S_{kk'}\bar{c}^{\,2}_{k'}\bar{c}^{*}_k+2T_{kk'}|\bar{c}_{k'}|^2\bar{c}_k), \tag{12}$$

where γ_k is the relaxation rate of mode k, $\Delta\omega_k=\omega_k-\omega_p/2$ is its detuning, and $\beta_{kk'}=q_k-q_{k'}$ is the phase difference between modes k and k'. Note that in an infinite medium $\alpha_{\Delta k}=0$ and Eq. (12) reduces to the same equation used in previous works.[19,20,26] In this condition we can multiply both sides of Eq. (12) by $\bar{c}_{-k}$, and using the symmetry $\mathbf{k},-\mathbf{k}$, we obtain the S equations[9,10] for the Cooper-pair variables σ_k:

$$\frac{1}{2}\frac{d\sigma_k}{dt}=-(\gamma_k+i\,\Delta\omega_k)\sigma_k-ih\rho_k n_k -i\sum_{k'}(S_{kk'}\sigma_{k'}n_k+2T_{kk'}n_{k'}\sigma_k), \tag{13}$$

where $\sigma_k=\bar{c}_k\bar{c}_{-k}=n_k\exp(i\phi_k)$, n_k being the number of magnons in mode $\mathbf{k}$ and ϕ_k the phase of the processing magnetization. The S equations have quadratic nonlinearities and in the polar form are very convenient for stability analysis. They have been used by many authors to study spin-wave turbulence and nonlinear dynamics. However, they are not suitable for finite samples because of the additional coupling between the spin-wave equations introduced by the $\alpha_{\Delta k}$ term.

The spin-wave equations (12) represent $2M$ (M is the number of nearly degenerate modes excited by the pump field) nonlinear differential equations of the form $d\mathbf{x}/dt=F(\mathbf{x},\boldsymbol{\mu})$, where $\mathbf{x}$ is the dynamical variable vector and $\boldsymbol{\mu}$ represents the (time-independent) parameters. The linearization[30] of the equations around the fixed points $\mathbf{x}_0$ given by $F(\mathbf{x}_0,\boldsymbol{\mu})=0$ yields $\mathbf{x}(t)=\mathbf{x}_0+\delta x\exp(\lambda t)$, where λ represents the eigenvalues of the Jacobian matrix $J_{ij}=\partial F_i/\partial x_j$. Physically, there are infinitely many modes involved as soon as the pumping exceeds the Suhl threshold, so that the problem of determining the eigenvalues is in principle immensely difficult. However, as Suhl and Zhang[17] have shown, the linearized equations have *collective,* normal-mode solutions, formed by linear superpositions of the spin-wave variables δx, each with an associated pair of complex eigenvalues λ. The character of the bifurcation is determined by the eigenvalues whose real part turns positive at the critical field h'_c, all others representing uninteresting damped solutions. In general, at not too intense driving, the dynamics is governed by essentially two modes, each resulting from the collective coupling of many spin-wave pair modes in a certain region of k space. It appears that each normal mode is described by an equation similar to that of individual k modes with parameters that are suitable averages of the values for the intervenient spin waves. This is justified by the fact that numerical calculations with only two modes have shown quite good qualitative agreement with the experimental observations.[13,14,19,26]

Our analysis of the auto-oscillations is based on the equations for two modes derived from Eq. (12):

$$\dot{c}_1=-(\gamma_1+i\Delta\omega_1)c_1-ih\rho_1(c^{*}_1+\alpha e^{i\beta/2}c^{*}_2) -i2(S_1c^2_1c^{*}_1+S_{12}c^{*}_1c^2_2+2T_{12}c_2c^{*}_2c_1), \tag{14}$$

$$\dot{c}_2=-(\gamma_2+i\Delta\omega_2)c_2-ih\rho_2(c^{*}_2+\alpha e^{-i\beta/2}c^{*}_1) -i2(S_2c^2_2c^{*}_2+S_{12}c^{*}_2c^2_2+2T_{12}c_1c^{*}_1c_2), \tag{15}$$

where the subscripts 1 and 2 denote the two collective modes, $S_k\equiv S_{kk}+2T_{kk}$, $\alpha\equiv\alpha_{\Delta k}$, $\beta\equiv\beta_{12}$, and the tilde in $\bar{c}_k$ was dropped to simplify the notation. Since c_k is complex, the set (14) and (15) represents four coupled equations. In the next section we show the results of numerical solutions of Eqs. (14) and (15) and of the diagonalization of the Jacobian matrix.

V. BIFURCATIONS OF THE SPIN-WAVE EQUATIONS

Although Eqs. (14) and (15) represent an enormous simplification of the original problem, they are still mathematically very complex. They have 12 independent parameters, so that a multitude of bifurcation phenomena can be encountered depending on the parameter values. In order to fully explore these phenomena, it is necessary to make use of numerical methods and integrate the equations in a computer. In the numerical studies with an arbitrary set of parameters, one usually finds that the solutions are attracted to stable fixed points. However, in certain regions of the parameter space, some fixed points become unstable and the solutions may exhibit a variety of dynamic behavior. Because of the complex nature of the modes involved in the dynamics, it is difficult to relate the parameters with the microscopic ones. However, we have found some sets of parameters that yield results very similar to those observed experimentally. This is done by solving Eqs. (14) and (15) numerically in a VAX 750 computer using a Runge-Kutta subroutine to obtain the steady-state time evolution of c_1, c_2, and the corresponding magnon occupation number $n_k=c^{*}_k c_k$. We also cal-

culate numerically the four eigenvalues λ of the Jacobian matrix of Eqs. (14) and (15) in order to investigate the nature of the auto-oscillation bifurcation. Since we want to work with quantities of order 1, the magnon number and interaction parameters are rescaled as $n_k \rightarrow F n_k$, $S_{kk'} \rightarrow F^{-1} S_{kk'}$, and $T_{kk'} \rightarrow F^{-1} T_{kk'}$, where $F = \omega_M / 4SN\gamma_k$. In YIG at room temperature, $\gamma_k \sim 2\times 10^6$ sec^{-1}, $\omega_M \simeq 3\times 10^{10}$ sec^{-1}, so that $F \sim 10^{17}$ in a sample with volume ~ 1 mm^3.

A. Hopf bifurcation

We consider initially a case of Hopf bifurcation obtained with the following parameters: $\Delta\omega_1 = \Delta\omega_2 = 0$, $\rho_1/\rho_2 = 0.7$, $\gamma_2/\gamma_1 = 5.0$, $S_1/\gamma_1 = -1.0$, $S_2/\gamma_1 = 0.5$, $S_{21}/\gamma_1 = 2.5$, $T_{21}/\gamma_1 = 1.125$, and $\alpha = 0$. These are the same parameters that give a chaotic dynamics qualitatively similar to one observed in experiments.[14,21] Note that the parameters are quite different for the two modes, indicating that they are degenerate modes far in k space. This justifies making $\alpha = 0$. In this case identical results were obtained with the two-mode equations derived from Eq. (13). Figure 9 shows the behavior of the trajectories projected on the $n_1 \times n_2$ plane, with increasing microwave pumping, represented by the control parameter $R \equiv h/h_{c_1}$. Figure 10 shows the behavior of the four corresponding Jacobian matrix eigenvalues in the complex plane with increasing R. Note that since mode 1 has lower relaxation rate γ_k and higher coupling ρ_k to the pumping, it has a lower Suhl threshold h_{c_1} and is excited first; so it is called the "strong mode." As the control parameter R increases in the range $1.0 < R \leq 2.4$, mode 1 is alone and the fixed point moves uniformly along the n_1 axis. In this range the eigenvalues corresponding to mode 1 are complex conjugate and move away from the real axis along the line $\mathrm{Re}\lambda = -\gamma_1$. The negative real

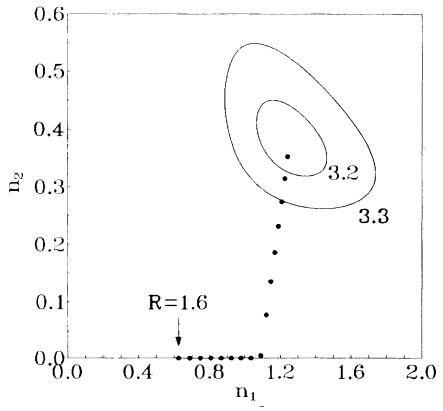

FIG. 9. Phase-space trajectories $n_1 \times n_2$ for the two-mode model, with increasing pumping $R = h/h_c$ in steps of 0.1. For $1.6 \leq R \leq 2.4$, the "strong mode" n_1 is alone. When R exceeds 2.4, a center manifold with $n_2 \neq 0$ ("weak mode") is born and the fixed point moves along the stable mode line. At $R \approx 3.17$, a Hopf bifurcation into a limit cycle occurs. The parameters used are the following: $\Delta\omega_1 = \Delta\omega_2 = 0$, $\rho_1/\rho_2 = 0.7$, $\gamma_2/\gamma_1 = 5.0$, $(S_{11} + 2T_{11})/\gamma_1 = -1.0$, $(S_{22} + 2T_{22})/\gamma_1 = 0.5$, $S_{12}/\gamma_1 = S_{21}/\gamma_1 = 2.5$, and $T_{12}/\gamma_1 = T_{21}/\gamma_1 = 1.125$.

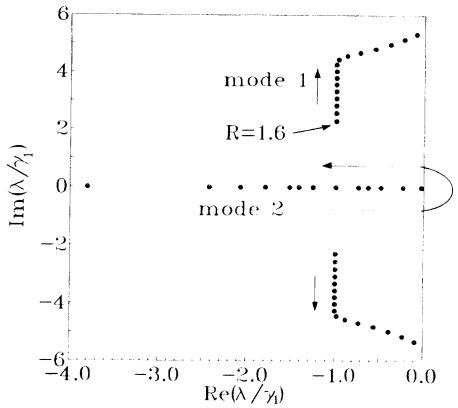

FIG. 10. Trajectories of the eigenvalues of the Jacobian matrix in the complex plane for the same parameters as in Fig. 9 with increasing pumping in steps of 0.1 in the range $1.6 \leq R \leq 3.1$.

part of the complex eigenvalues characterizes the fixed point $n_1 \neq 0$, $n_2 = 0$ as a focus attractor. In this range of R, mode 2 has two real and negative eigenvalues moving toward the origin.

At $R^* \approx 2.4$ (actually 2.394 566 according to the theoretical prediction[31]), there is a zero-eigenvalue bifurcation. At this point the eigenvalue for mode 2 moving on the real axis in the positive direction reaches zero, turning the direction of motion to negative values with further increase in R. At this point a center manifold with $n_2 \neq 0$ is born (Fig. 9), and the complex eigenvalues initially moving on the line $\mathrm{Re}\lambda = -\gamma_1$ sharply turn direction and begin to move toward the imaginary axis (Fig. 10) as R exceeds R^*. In the range $R^* < R < R_c'$, both weak and strong modes are excited at steady-state values. As R increases, the fixed point $n_1 \neq 0$, $n_2 \neq 0$ moves along the stable-mode line shown in Fig. 9. At $R = R_c' \approx 3.17$ a pair of complex conjugate eigenvalues crosses the imaginary axis, the fixed point becomes unstable, and a Hopf bifurcation into a limit cycle occurs. This corresponds to the onset of the auto-oscillations with a finite frequency $f_0/\gamma_1 = \mathrm{Im}\lambda/2\pi\gamma_1 \simeq 0.87$ and vanishing amplitude. As R increases beyond R_c', the amplitude follows the scaling law $A \sim (R - R_c')^{1/2}$, as in the experimental observations of Fig. 5.

B. Homoclinic bifurcation

Quite different bifurcation may occur in the spin-wave equations with other sets of parameters. Let us examine numerically two modes with the same parameters used in Ref. 19: $\Delta\omega_1 = (-2\pi)0.3$, $\Delta\omega_2 = (2\pi)0.2$ (in units of $\gamma_1 = 10^6$ sec^{-1}), $S_{11} = S_{22} = S_{12} = 4.078$, $T_{11} = T_{22} = -1.896$, $T_{12} = 0$, $\rho_1 = \rho_2$, $\gamma_1 = \gamma_2$, and $\alpha = 0$. In this case, in the absence of spin-wave interaction, the Suhl thresholds are $R_{c1} \equiv \rho_1 h_{c_1}/\gamma_1 = 2.133$ and $R_{c2} = 1.604$, so that 1 is the weak mode and 2 is the strong mode. Mode 2 has a one-dimensional unstable manifold for $R > 1.604$, a value for which it becomes a saddle point, while mode 1 at the origin is a spiral focus. This at first sight suggests a Silnikov homoclinic recurrence.[30] Since the recurrent be-

havior is found as soon as one of the modes becomes unstable, we have a situation of homoclinic bifurcation with nonhyperbolic equilibria[32] instead of a Hopf bifurcation.

The results of the numerical study are presented in Figs. 11–13. Figure 11 shows that as the pumping increases beyond $R \simeq 1.64$, very-low-frequency aperiodic spiking behavior develops in the amplitude n_1 of the weak mode. The (average) frequency increases rapidly with R, contrasting with the lack of variation in the Hopf bifurcation. Moreover, in striking similarity with the experimental observation of Fig. 6, the "oscillation" sets in with finite amplitude, as in a first-order phase transition. Figure 12 shows the trajectory in phase space projected on the $\mathrm{Re}(c_1)\times\mathrm{Im}(c_1)$ plane for $R=1.685$. The stroboscopic sampling at $\sim\frac{1}{400}$ of the period indicates that c_1 describes a slow spiral motion around the origin before escaping for a fast journey away from the origin, giving rise to the spiking behavior. Finally, Fig. 13 shows the trajectories of the four eigenvalues of the Jacobian matrix with increasing R. Note that the bifurcation occurs when the imaginary axis is crossed by a real eigenvalue, quite differently from the Hopf scenario of Fig. 10. This is consistent with the very low frequency of the spiking oscillation observed in Fig. 11 near the bifurcation. Note also that only at higher pumping levels $R>1.8$ do the auto-oscillations behave as described in Figs. 3 and 9 of Ref. 19. In closing this section, we mention that other types of bifurcation phenomena have been found in the spin-wave equations, such as one zero-two imaginary eigenvalue codimension-two bifurcations and transverse and tangent homoclinic phenomena near the Hamiltonian limit.[31]

VI. NON-MOMENTUM-CONSERVING PUMPING IN FINITE-SIZE SAMPLES

In the numerical examples of last section, we considered $\alpha=0$, which reduces Eqs. (14) and (15) to the same as those for an infinite medium. In this section we show that with $\alpha\neq 0$ our model accounts for some important quantitative features of the auto-oscillations observed experimentally not obtained with $\alpha=0$; namely, the threshold for bifurcation h_c' is only slightly higher than the SI threshold h_c; the frequency can be quite lower than the spin-wave relaxation rate; and for some configurations the frequency and threshold difference $h_c'-h_c$ vary approximately inversely proportional to the sample diameter and linearly with the wave number k.

In order to demonstrate the effect of the momentum symmetry-breaking term in the spin-wave pumping, let us consider initially the same parameters used by Nakamura, Ohta, and Kawasaki[10] in one of the earliest numerical applications of the two-mode model: $\Delta\omega_1/\gamma_1=\Delta\omega_2/\gamma_1=-1.0$, $\gamma_1=\gamma_2$, $\rho_1=\rho_2$, $S_1/\gamma_1=S_2/\gamma_1=1.0$, $S_{12}/\gamma_1=-0.4$, and $T_{12}/\gamma_1=-0.75$. With $\alpha=0$ the threshold for auto-oscillation is $R_c'\simeq 3.65$. Figures 14(a) and 14(b) show, respectively, the trajectory

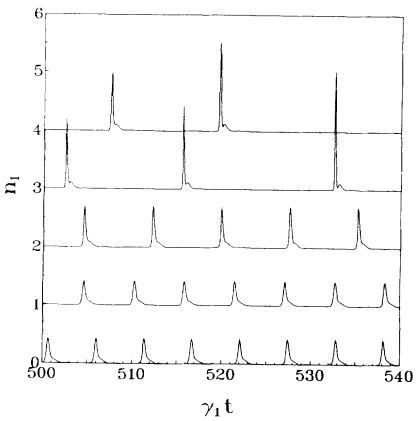

FIG. 11. Numerical solutions of the two-mode model with parameters $\Delta\omega_1=-2\pi\times 0.3$, $\Delta\omega_2=2\pi\times 0.2$, $S_{11}=S_{22}=S_{12}=4.078$, $T_{11}=T_{22}=-1.896$, $T_{12}=0$, $\rho_1=\rho_2$, $\gamma_1=\gamma_2$, and $R=1.66$, 1.67, 1.68, 1.69, and 1.70 from top to bottom. Note that the frequency grows rapidly with increasing pumping level and the amplitude sets in with a finite value, similar to the experimental observation of Fig. 6.

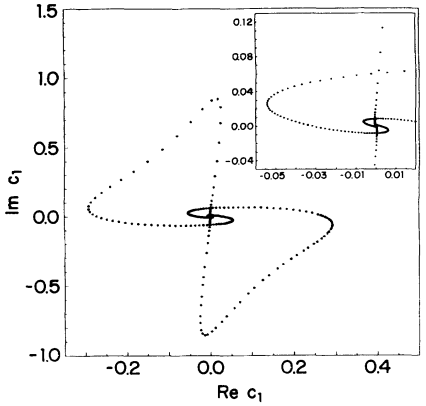

FIG. 12. Phase-space trajectories $\mathrm{Re}(c_1)\times\mathrm{Im}(c_1)$ with the same parameters of Fig. 11 and $R=1.685$. The stroboscopic sampling indicates the slow spiral motion around the origin and a fast journey away from the origin. The inset shows the magnified region around the origin.

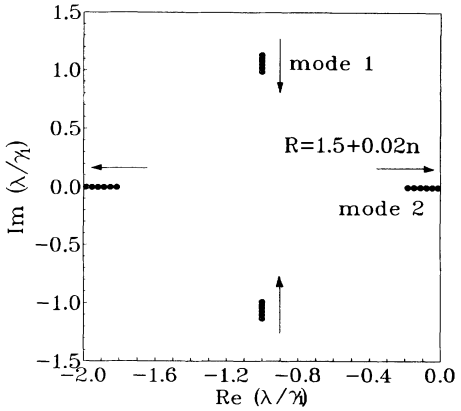

FIG. 13. Trajectories of the eigenvalues of the Jacobian matrix for the same parameters of Fig. 11, with $1.5\leq R\leq 1.6$. The bifurcation occurs when the real eigenvalue crosses the imaginary axis. This is consistent with very low frequency of the spikes observed in Fig. 11 and in the experimental traces in Fig. 6.

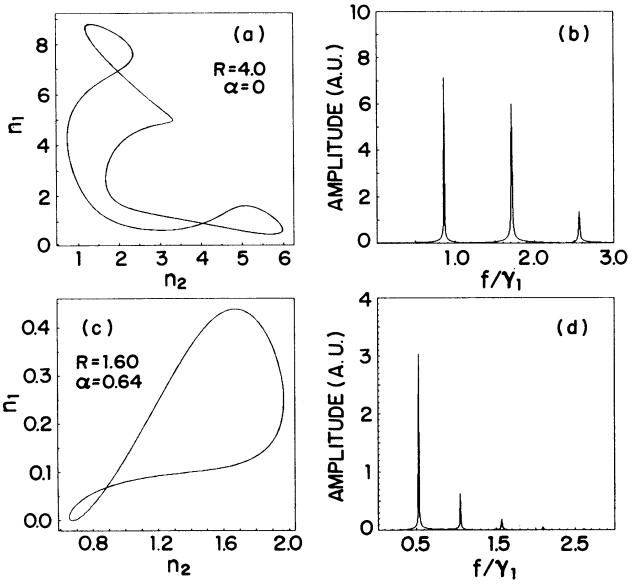

FIG. 14. Comparison of the trajectories in phase space $n_2 \times n_1$ and the corresponding spectra for n_1 for pumping (a) and (b) in an infinite medium and (c) and (d) in a finite-size sample. The parameters are the same as in Ref. 10, $\Delta\omega_1=\Delta\omega_2=-1.0$, $S_1=S_2=1.0$, $S_{12}=-0.4$, $T_{12}=-0.75$, $\gamma_1=\gamma_2$, and $\rho_1=\rho_2$.

in phase space $n_2 \times n_1$, for $R=4.0$, and the corresponding Fourier spectrum of $n_1(t)$. With these parameters the threshold is much higher than the experimental ones, normally in the range $R_c' \sim 1.1-2.0$, as in Figs. 2 and 3. The auto-oscillation frequency is $f_0 \simeq \gamma_1$, which corresponds to at least 1 MHz in YIG. This is 2–10 times higher than the typical experimental values, as seen in Figs. 2–6. If we now make $\alpha=0.64$ ($\simeq 2/\pi$) and $\beta=0$, the bifurcation threshold is reduced to $R_c' \simeq 1.45$ and the frequency decreases to $f_0 \simeq \gamma/2$, as shown in Fig. 14(d), approaching the experimental values.

In the example above we chose for α the largest possible value, $2/\pi \simeq 0.64$, because it minimizes the auto-oscillation threshold. This value is appropriate for the pumping of two neighboring standing waves along the [100] crystal direction. In the case of β, it is not possible to know *a priori* which value it should have. If the two modes were pumped independently, i.e., $\alpha=0$, the value of β would be immaterial. However, with $\alpha \neq 0$, β becomes a relevant parameter. This is demonstrated in Fig. 15, which shows the complex eigenvalues λ for several values of β at two pumping intensities $R=1.18$ and 1.24, $\alpha=0.64$, the other parameters being the same as in Fig. 14. The value of β for which a pair of complex eigenvalues crosses the imaginary axis first is $\beta \simeq 60°$. This occurs at the threshold $R_c' \simeq 1.25$, a value smaller than with $\beta=0$. At this threshold there is a Hopf bifurcation leading to self-oscillation with frequency $f_0/\gamma_1 = \mathrm{Im}\lambda/2\pi\gamma_1 \simeq 0.5$. Hence the phase difference β between the two neighboring modes in **k** space adjusts itself in order to minimize the self-oscillation threshold. The numerical study has shown that this value depends on the set of parameters, and it usually leads to a low threshold value R_c'.

Finally, let us demonstrate how the model accounts for

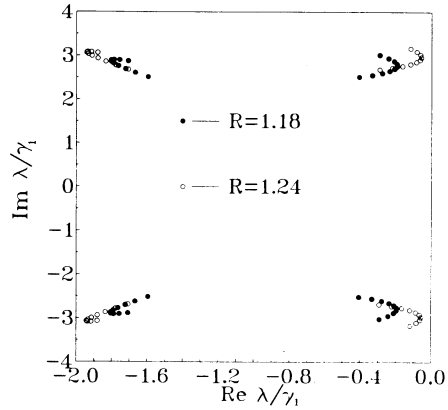

FIG. 15. Behavior of the eigenvalues of the Jacobian matrix with the phase difference β varying from 0° to 90° in steps of 10°, for two pumping intensities $R=1.18$ and 1.24. The parameters are the same as in Fig. 14 with $\alpha=0.64$.

the dependence of the auto-oscillation frequency and threshold on the wave number k and sample diameter d. These quantities enter Eqs. (14) and (15) through the detunings $\Delta\omega_k$ of the two neighboring modes involved in the dynamics. In order to conserve energy within an uncertainty of the order of the relaxation rate, we take $\Delta\omega_1$ and $\Delta\omega_2$ with opposite signs and magnitudes smaller than γ_1. Equations (14) and (15) were solved for several parameter sets with $\alpha \neq 0$ and varying frequency spacing $\Delta\omega=|\Delta\omega_1-\Delta\omega_2|$. The results reveal that with $\alpha \neq 0$ the auto-oscillation frequency and threshold normally depend on $\Delta\omega$. This is illustrated in Fig. 16 for the following parameters: $\Delta\omega_1=-2\Delta\omega/3$, $\Delta\omega_2=\Delta\omega/3$, $S_1/\gamma_1=S_2/\gamma_1=0.8$, $S_{12}/\gamma_1=0.35$, $T_{12}/\gamma_1=-0.01$, $\gamma_1=\gamma_2$, $\rho_1=\rho_2$, $\alpha=0.64$, and $\beta=\pi$ (which is the value that minimizes R_c'). The auto-oscillation frequency at the Hopf bifurcation as well as the threshold R_c' clearly depends on the frequency spacing. The computed frequency for values of $\Delta\omega$ in the range $0 \leq \Delta\omega/\gamma_1 \leq 1.0$ is found to follow approximately a linear dependence,

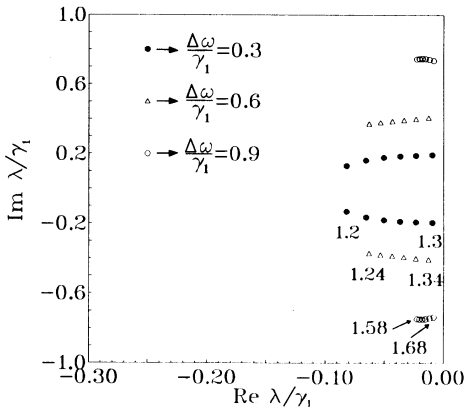

FIG. 16. Trajectories of the eigenvalues with increasing pumping in steps of 0.01 for several values of the frequency spacing $\Delta\omega$ between the two modes. The parameters are $\Delta\omega_1=-2\Delta\omega/3$, $\Delta\omega_2=\Delta\omega/3$, $S_1=S_2=0.8$, $S_{12}=0.35$, $T_{12}=-0.01$, $\gamma_1=\gamma_2$, $\rho_1=\rho_2$, $\alpha=0.64$ and $\beta=\pi$. Note that the auto-oscillation frequency and threshold for bifurcation increase approximately linearly with $\Delta\omega$.

$f_0/\gamma_1 = a + b\Delta\omega/\gamma_1$, where the coefficients a and b depend on the parameter values. For some sets of parameters, the results give $b=0$; hence the frequency does not depend on $\Delta\omega$. This explains why in the experiments some modes display a size dependence in the frequency while others do not. It all depends on the parameters of the modes involved in the dynamics.

The relation between f_0 and d is based on the fact that the frequency spacing between neighboring modes is $\Delta\omega = \pi v_g/d$. For values of k in the range of our experiments, both v_g and γ_k vary linearly with k. Therefore the prediction of our model for the auto-oscillation frequency is

$$f_0/\gamma_k \simeq a' + b'k/d \ . \tag{16}$$

The solid curves in Fig. 8 are fits to this expression using for all spheres the same values for b' but different values for a', as indicated in the caption. Although outside the range of k in Fig. 8 the data points depart from this fit, the agreement between the model and data is impressive. A result similar to (16) is obtained for the threshold difference $R_c' = R_c$, in agreement with the data of Fig. 7.

VII. CONCLUSIONS

In this paper we presented a detailed experimental and theoretical investigation of the self-oscillations generated by the microwave pumping of spin-wave instabilities in YIG spheres. The experiments reveal interesting features; namely, the self-oscillations originate in a variety of bifurcations, two commonly observed types being Hopf and homoclinic, and the threshold field and onset frequency of the self-oscillations originating in a Hopf bifurcation depend on the pumping configuration, wave number, and relaxation rate of the spin-wave modes involved and on the sample diameter.

These observations have been explained quantitatively with a theoretical model for interacting plane spin waves. The model is based mostly on results obtained by previous authors, but it contains an additional non-momentum-conserving pumping term due to the finiteness of the sample size. This term reduces considerably the self-oscillation threshold field h_c' and frequency f_0 consistent with experiments. In addition, it introduces a dependence of these quantities on wave number k and sample diameter d in quite good agreement with data.

Finally, let us summarize our understanding of the origin of the self-oscillations. As the microwave pumping field exceeds the threshold for parametric spin-wave excitation h_c, many modes are pumped with population (10^{17}) much higher than the thermal values ($\sim 10^3$). If the field is not much higher than h_c, these modes are degenerate with frequency $\omega_k \simeq \omega_p/2$ and propagate at an angle close to that of the SI threshold, $\theta_k = \pi/2$ in parallel pumping and $\theta_k = \pi/4$ in subsidiary resonance for fields $H_0 < H_c$. Initially, all the modes are at steady-state values, corresponding to fixed-point solutions of the spin-wave equations. However, at such high populations, the effective microwave field that each mode exerts on the others due to the magnon-magnon interaction competes in intensity with the direct microwave pumping of those modes and tends to create an instability. Although all the modes are standing waves, the phase differences between the traveling waves in each pair assume a random value, so that the spatial distribution of the magnetization is uniform throughout the sample.

As the pumping field is increased further beyond a second threshold h_c', an instability develops, now between the parametric spin-wave modes. This corresponds to the crossing of the imaginary axis by one or more eigenvalues of the Jacobian matrix describing the spin-wave system. Above this threshold there is a collective mode of the system, oscillating with a small frequency that has no direct connection with the microwave pumping frequency. This picture is essentially the same as the one presented by Suhl and Zhang.[17] The contribution of this paper comes next.

Not all of the nearly degenerate modes with $\omega_k \simeq \omega_p/2$, or even those pumped above threshold, become involved in the dynamics of the self-oscillation. This is so because the spin-wave interaction parameters vary considerably in magnitude and sign in the spin-wave manifold, especially with the propagation angle θ_k. Thus only the modes in some small regions in k space will have the nonlinear parameters appropriate for the lowest auto-oscillation threshold. As we showed in Sec. VI, the threshold for auto-oscillation is reduced considerably when one considers the pumping of spin-wave pairs with opposite wave vectors differing by π/d, in addition to the usual pumping of pairs with equal wave vectors. Therefore the modes involved in the dynamics of the auto-oscillation are comprised of groups of spin waves, each two individual waves with wave vectors differing by π/d. The presence of each wave in the pumping term of the other represents a modulation with frequency proportional to the frequency difference $\Delta\omega$. As a result, a self-oscillation regime is established with frequency proportional to $\Delta\omega$ and spatial distribution of the type $\cos(\pi x/d)$. The results of the numerical solutions of the modified spin-wave equations for two neighboring modes agree very well with the experimental observations. In particular, we call attention to the following features: (1) The auto-oscillation frequency at the threshold h_c' varies approximately linearly with the wave number k and inversely with the sample diameter. (2) A similar dependence is obtained for the threshold difference $h_c' - h_c$. (3) The frequency depends not only on k and d, but also on the nonlinear parameters. This is clear in the comparison of Figs. 15 and 16, which show that by changing the parameters, the frequency can vary by an order of magnitude, 10^{-1}–10^0 in units of the relaxation rate γ_k.

ACKNOWLEDGMENTS

The authors acknowledge Dr. Flavio M. de Aguiar for many contributions earlier in our research program and Professor Jair Koiller and Dr. Ana Cascon for many suggestions and discussions regarding bifurcations. This work was partially supported by Financiadora de Estudos e Projetos, Conselho Nacional de Desenvolvimento Científico e Tecnológico, Coordenação do Aperfeiçoamento do Pessoal de Nível Superior e Fundação de Amparo à Ciência e Tecnologia de Pernambuco.

[1]R. W. Damon, Rev. Mod. Phys. **25**, 239 (1953).
[2]N. Bloembergen and S. Wang, Phys. Rev. **93**, 72 (1954).
[3]H. Suhl, J. Phys. Chem. Solids **1**, 209 (1957).
[4]F. R. Morgenthaler, J. Appl. Phys. **31**, 95S (1960).
[5]E. Schloman, J. J. Green, and U. Milano, J. Appl. Phys. **31**, 386S (1960).
[6]T. S. Hartwick, E. R. Peressini, and M. T. Weiss, J. Appl. Phys. **32**, 223S (1961).
[7]S. Wang, G. Thomas, and Ta-Lin Hsu, J. Appl. Phys. **39**, 2719 (1968).
[8]G. Thomas and G. Komoriya, J. Appl. Phys. **46**, 883 (1974).
[9]V. S. L'vov, S. L. Musher, and S. S. Starobinets, Zh. Eksp. Teor. Fiz. **64**, 1074 (1973) [Sov. Phys.—JETP **37**, 546 (1973)]; V. E. Zakharov, V. S. L'vov, and S. S. Starobinets, Usp. Fiz. Nauk **114**, 609 (1974) [Sov. Phys. Usp. **17**, 896 (1975)]; V. I. Ozhogin and A. Yu. Yakubovskii, Z. Eksp. Teor. Fiz. **67**, 287 (1974) [Sov. Phys. JETP **40**, 144 (1975)].
[10]K. Nakamura, S. Ohta, and K. Kawasaki, J. Phys. C **15**, L143 (1982).
[11]G. Gibson and C. Jeffries, Phys. Rev. A **19**, 811 (1984).
[12]F. Waldner, D. R. Barberis, and H. Yamazaki, Phys. Rev. A **31**, 420 (1985).
[13]S. M. Rezende, F. M. de Aguiar, and O. F. de Alcantara Bonfim, J. Magn. Magn. Mater. **54-57**, 1127 (1986); Phys. Rev. B **33**, 5153 (1986).
[14]F. M. de Aguiar and S. M. Rezende, Phys. Rev. Lett. **56**, 1070 (1986).
[15]A. I. Smirnov, Zh. Eksp. Teor. Fiz. **90**, 385 (1986) [Sov. Phys. JETP **63**, 222 (1986)].
[16]H. Yamazaki, M. Mino, H. Nagashima, and M. Warden, J. Phys. Soc. Jpn. **56**, 742 (1987).
[17]H. Suhl and X. Y. Zhang, Phys. Rev. Lett. **57**, 1480 (1986); Phys. Rev. B **38**, 4893 (1988).
[18]S. P. Lim and D. L. Huber, Phys. Rev. B **37**, 5426 (1988).
[19]P. H. Bryant, C. D. Jeffries, and K. Nakamura, Phys. Rev. Lett. **60**, 1185 (1988); Phys. Rev. A **38**, 4223 (1988).
[20]H. Yamazaki and M. Mino, Prog. Theor. Phys. Suppl. **98**, 400 (1989).
[21]S. M. Rezende, F. M. de Aguiar, and A. Azevedo, Phys. Rev. B **39**, 9448 (1989).
[22]M. Mino, H. Yamazaki, and K. Nakamura, Phys. Rev. B **40**, 5279 (1989).
[23]T. L. Carroll, F. J. Rachford, and L. M. Pecora, Phys. Rev. B **38**, 2938 (1988).
[24]M. Warden and F. Waldner, J. Phys. (Paris) Colloq. **49**, C8-1573 (1988).
[25]R. D. McMichael and P. E. Wigen, Phys. Rev. Lett. **64**, 64 (1990).
[26]S. M. Rezende and F. M. de Aguiar, Proc. IEEE **78**, 893 (1990); Physica A **163**, 232 (1990).
[27]S. M. Rezende, F. M. de Aguiar, and A. Azevedo, J. Appl. Phys. **67**, 5624 (1990).
[28]S. M. Rezende, A. Azevedo, A. Cascon, and J. Koiller, J. Appl. Phys. **69**, 5430 (1991).
[29]C. E. Patton and W. Jantz, J. Appl. Phys. **50**, 7082 (1979).
[30]See J. Guckenheimer and P. Holmes, *Nonlinear Oscillations, Dynamical Systems, and Bifurcations of Vector Fields* (Springer-Verlag, New York, 1983).
[31]A. Cascon, J. Koiller, and S. M. Rezende Physica D (to be published).
[32]B. Deng, SIAM J. Math. Anal. **21**, 693 (1990).

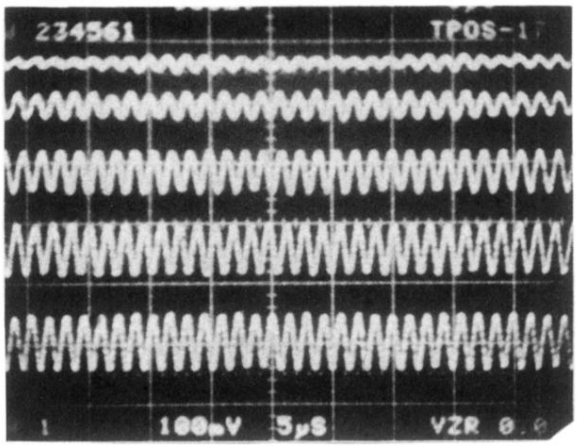

FIG. 4. Oscilloscope traces showing the behavior of the auto-oscillation with increasing microwave field $R = h/h_c$ in parallel pumping with a YIG sphere oriented along [111], $H_0 = 1570$ Oe, $f_p = 9.5$ GHz. The time scale is 5 μs per division, and $R = 1.224$, 1.255, 1.293, 1.321, and 1.342 from top to bottom. The constant frequency and rapid growth in the amplitude characterize a Hopf bifurcation.

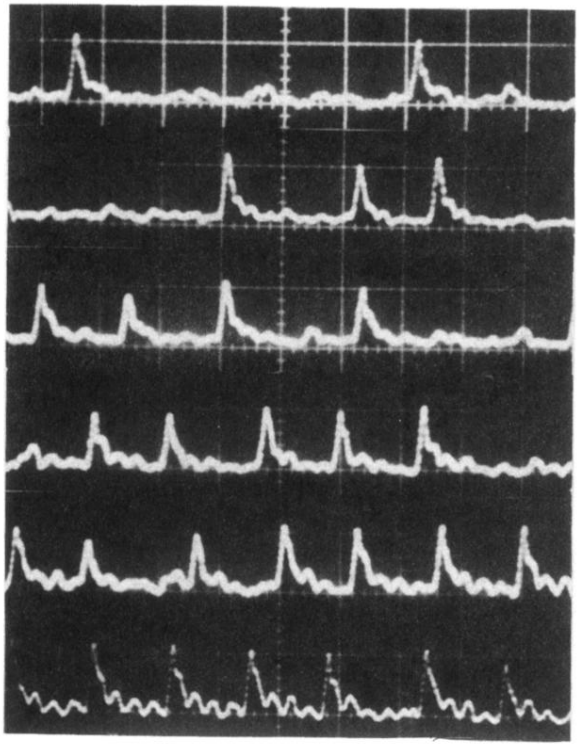

FIG. 6. Oscilloscope traces of the auto-oscillation obtained with subsidiary-resonance pumping with increasing microwave field $R = h/h_c$ in a YIG sphere oriented along [110], $H_0 = 1950$ Oe, $f_p = 9.4$ GHz. The time scale is 10 μs per division $R = 1.862$, 1.872, 1.883, 1.894, 1.905, and 1.916 from top to bottom. Note that the auto-oscillation sets in with a finite amplitude and rapidly increasing frequency, quite differently from the Hopf scenario of Fig. 4.